

UCSF

UC San Francisco Electronic Theses and Dissertations

Title

Evaluating EPflex MRline Guidewire for Endovascular Interventions Guided by MRI at 3T vs. X-ray Fluoroscopy

Permalink

<https://escholarship.org/uc/item/0xp65544>

Author

Williams, Jack Clark

Publication Date

2019

Peer reviewed|Thesis/dissertation

Evaluating EPflex MRline Guidewire for Endovascular Interventions Guided by MRI at
3T vs. X-ray Fluoroscopy

by
Jack Williams

THESIS

Submitted in partial satisfaction of the requirements for degree of
MASTER OF SCIENCE

in

Biomedical Imaging

in the

GRADUATE DIVISION

of the

UNIVERSITY OF CALIFORNIA, SAN FRANCISCO

Approved:

DocuSigned by:

Steven Hetts

Steven Hetts

DA41E0D34A4A463...

Chair

DocuSigned by:

Alastair Martin

Alastair Martin

DocuSigned by:

Janine Lupo

Janine Lupo

DocuSigned by:

Daniel Cooke

Daniel Cooke

65454CD34FB442F...

Committee Members

Copyright 2019

by

Jack Williams

Acknowledgements

I would like to thank everyone who provided guidance and participated in this project. First, thanks to my project advisory committee members Dr. Steven Hetts, Dr. Daniel Cooke, Dr. Alastair Martin, and Dr. Janine Lupo. Additional thanks to Dr. Caroline Jordan, Bridget Kilbride, Dr. Aaron Losey, Parth Kumar, and Teri Moore for all your help, advice, and support.

Evaluating EPflex MRline Guidewire for Endovascular Interventions Guided by MRI at 3T vs. X-ray Fluoroscopy
By Jack Clark Williams

Abstract

This project sought to evaluate the efficacy of using the EPflex MRline guidewire for endovascular treatment guided by real-time Magnetic Resonance Imaging (MRI). MRI theoretically has numerous advantages over x-ray, the current clinical standard imaging modality for endovascular procedures. The most profound advantage of MRI is the ability to acquire physiological functional information, via perfusion and diffusion measures, for better intervention planning before and during the procedure. The EPflex guidewire was selected because of its ability to perform in an MRI and x-ray fluoroscopy environment, allowing for relevant and useful comparisons of the guiding imaging modality. An abdominal aorta phantom was used to assess the ability of experienced and inexperienced operators to successfully navigate the wire under each imaging modality. It was found that x-ray guidance provided statistically faster and more successful navigation attempts than MRI guidance; however, more clinical tests need to be performed in order to assess the clinical significance of these results. This study represents an important step in the direction of developing safer and more effective imaging systems for guiding endovascular procedures.

Table of Contents

Introduction.....	1
Overview.....	1
Hypothesis.....	2
Methods	3
Overview.....	3
EPflex MRline Guidewire.....	3
RTHawk Software	4
Phantom Model	7
MRI Guidance Procedures	8
X-ray Guidance Procedures	10
Statistical Analysis	11
Results	11
Discussion.....	16
Conclusion	19
References.....	20

List of Figures

Figure 1.....	4
Figure 2.....	4
Figure 3.....	5
Figure 4.....	7
Figure 5.....	8
Figure 6.....	10
Figure 7.....	14
Figure 8.....	14
Figure 9	15
Figure 10.....	15

List of Tables

Table 1	12
Table 2	13
Table 3	13

Introduction

Overview

There is currently a movement to develop clinically useful and reliable methods to perform endovascular treatment guided by real-time Magnetic Resonance Imaging (MRI) [1-7]. Endovascular treatment within the field of Interventional Radiology (IR) currently uses x-ray fluoroscopy as the standard modality to guide the procedures and allow visualization of the instruments within patient circulation [8]. Previously, it was demonstrated that real-time MRI was not capable of offering adequate frame rates of image acquisition to guide IR procedures [5]. However, MRI software platforms have recently been introduced (RTHawk, HeartVista Inc., Los Altos, CA) and real-time MRI sequences have emerged (i.e. T-SENSE and T-GRAPPA). These advances provide renewed hope for MRI guidance of endovascular procedures [10].

MRI has advantages over x-ray fluoroscopy in several vital aspects of treatment, starting with the ability to obtain functional information such as perfusion and diffusion that x-ray cannot provide [6]. The acquisition of diffusion and perfusion information is the most definitive advantage of using MRI as the guiding modality for endovascular treatment. As it pertains to MRI, diffusion refers to the random Brownian motion of water particles moving through tissue. In a diffusion MR image, every voxel represents the displacement distribution of water molecules within that voxel [12]. It has been shown that the degree of water diffusion in a voxel decreases during an ischemic event and can be used to identify dead cells [16]. This phenomenon provides data necessary for planning endovascular treatment such as identifying regions of viable brain tissue in the case of stroke treatment to determine if an intervention would be beneficial [12]. Additionally, MRI does not use ionizing radiation to create an image, which can be harmful

to the patient and operating room (OR) staff. The peak skin dose of radiation in some x-ray guided IR procedures may be sufficient to cause detrimental effects on the skin of the patient [9].

The use of MRI to guide IR procedures would also eliminate the need to change hospital rooms in the case of stroke treatment. In the traditional treatment of stroke, the patient presents to the emergency department and is sent for an MRI or Computed Tomography (CT) scanning session to evaluate brain condition with perfusion imaging. The images are analyzed, and if an intervention is necessary, the patient is taken to a specialized angiography suite for x-ray-guided thrombectomy [17]. Changing rooms wastes valuable time, so the ability to diagnose and treat in the same MRI suite would be beneficial.

Overall, the flexibility of MR image contrast is appealing for procedure guidance, but there are unique challenges that require a specialized environment [13]. As we prepare for the future of MRI-guided intervention, a host of new equipment is needed to facilitate the new interventional environment. MRI employs three main magnetic fields to create images. The gradient system, used for spatial encoding, involves rapidly changing magnetic fields that could impact devices and produce nerve stimulation. The strong static magnetic field (B_0) requires the use of non-ferromagnetic instruments. Radiofrequency (RF) pulses can cause locally elevated heating on long conductive structures, which has implications on the length and type of guidewires and catheters that can be used. To achieve clinical utility in an MR environment, catheters and guidewires must MRI-safe and must also be readily visualized on MR images.

Hypothesis

Novel endovascular devices and real-time MRI methods are now sufficiently advanced to produce navigation capabilities that are comparable to conventional x-ray imaging. We aim to

test this hypothesis by testing experienced and inexperienced practitioners' ability to navigate an endovascular device through a vascular phantom while using either real-time MRI or conventional x-ray guidance.

Methods

Overview

This study used a simple, non-flowing abdominal aorta phantom model to test the navigability of a novel guidewire into phantom renal artery branches in the coronal plane. Two attending interventionalists and two inexperienced operators attempted to navigate a given guidewire into each phantom renal artery using x-ray fluoroscopy and MRI to guide the procedures. Success rates and navigation times were measured and analyzed. A successful run was counted if the operator navigated wire from the base of the phantom aorta into one of the renal arteries in less than 60 seconds. A failure was counted if a navigation attempt exceeded 60 seconds.

EPflex MRline Guidewire

A schematic of the EPflex MRline guidewire (Feinwerktechnik GmbH, Dettingen an der Erms, Germany) used in this study is shown in Figure 1. The wire dimensions were 0.035" in diameter and 150cm in length. The "MRI marker" shown on the figure is made of iron-platinum nanoparticles and causes local intravoxel dephasing of the B_0 magnetic field near the marker. The main core of the wire is made of a high-strength polymeric material. Figure 2 shows the B_0 field inhomogeneities created by different markers on different guidewires with the EPflex guidewire denoted by the red arrow. These inhomogeneities appear as a loss of signal in the vicinity of the marker due to intravoxel dephasing [3]. This passive disruption of the B_0 field is

in contrast to devices with “active” markers that incorporate MRI receive coils or antenna and a conductive connection to the MRI scanner to create device contrast to background tissue [8].

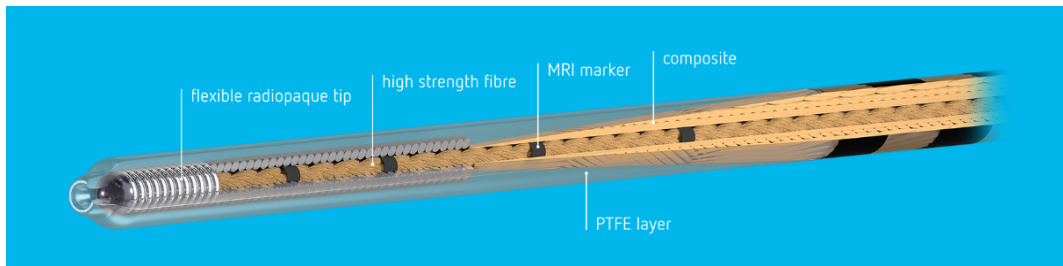


Figure 1

This is a schematic representation of EPflex MRline guidewire. [11]

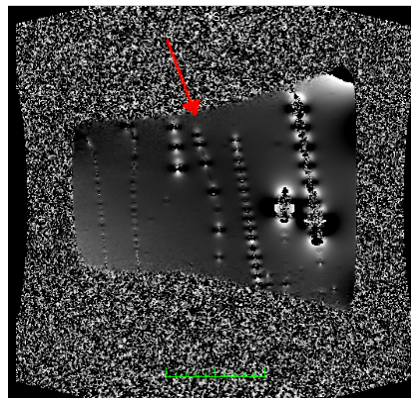


Figure 2

This phase image demonstrates the B0 field inhomogeneity created by passive markers on guidewires. The EPflex wire is denoted by the red arrow.

The EPflex guidewire tested in this study was developed to be used in an x-ray and MRI environment in order to better develop and compare the two imaging modalities.

RTHawk Software

Using MRI to guide precise endovascular intervention requires a very high rate of image acquisition to allow the safe movement of catheters and guidewires within a patient’s vasculature. Fast acquisition rate is difficult to attain due to the nature of MRI acquisition. Raw MRI data, called k -space, is collected line-by-line in the frequency domain, which requires multiple RF pulses for a single image. Basic MR image production, where each RF pulse

corresponds to a single line of k -space, can take several minutes, however special k -space acquisition protocols can be employed to achieve high acquisition framerates for MRI. RTHawk was developed for the purpose of simplifying MRI acquisition and allowing for real-time (roughly three images per second) image collection and display. The paper published by Santos et al. describes the operation and development of the real-time software which will be summarized as follows.

RTHawk provides high flexibility and performance to enable new and computationally demanding tasks, the most notably being high framerate reconstruction and on-the-fly reconfiguration of MR scanning protocols. RTHawk employs a network protocol designed to communicate with the data acquisition and the pulse sequence modulator of the scanner. This network also allows the workstation to issue and receive commands about the pulse sequence parameters. The reconstruction system was developed using a “high quality and high speed gridding based reconstruction algorithm” which pre-calculates the gridding convolution and uses a “sliding window” method described by Riederer et al. Since the data is reconstructed as it arrives, a new frame is generated for each acquisition. Figure 3 represents a schematic of the gridding process employed by RTHawk.

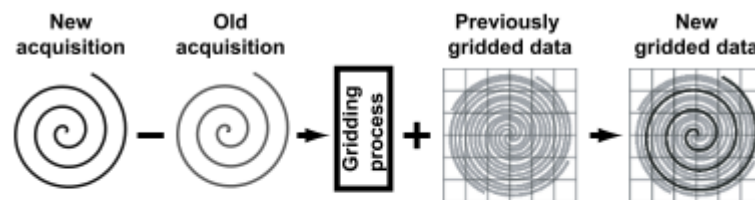


Figure 3

Sliding window reconstruction. Corresponding view is saved and is subtracted from the new acquisition. The difference is gridded and added to the previously reconstructed image [14]

The sliding window reconstruction method functions by allowing consecutive image frames to share k -space data so that an entire k -space grid is not reconstructed for each image [15]. Figure 4A illustrates a pulse sequence for a common echo planar imaging protocol with several RF pulses required for a single image. Figure 4B shows a Spoiled Gradient Recalled Echo (SPGR) sequence from which the sliding window sequence is based, and Figure 4C shows the sliding window pulse sequence. The modification of the SPGR sequence to achieve a sliding window is done by first reducing the number of phase encoding steps and/or the repetition time (TR) by increasing the bandwidth of the readout or reducing the number of readout points. A “window” with a width equal to the number of phase encoding steps is then “slid” along the acquired data and only the measurements within the window are used for reconstruction. As illustrated by the example in Figure 4C, only two new phase encodings are used for each subsequent image display and the rest are reused from the previous display. Note that the first image display uses phase encodings 1-48, while the second image display, a mere 33msec later, uses phase encodings 3-2’. This method essentially decouples the acquisition time of one distinct image from the time between successive images in a sequence [15]. By applying sliding window strategies, we can speed up frame rates above the true image acquisition time. Thus, while a single full image could take 250-1000ms to acquire, the sliding window approach could allow for frame rates in the 30ms/image range. High speed reconstruction from the sliding window is also possible because it is not necessary to perform full 2D Fourier transform reconstructions for every phase encoding. The contribution of the first two new phase encodes (1’ and 2’) can be determined individually and added to the first displayed image while the contributions of the original encodes 1 and 2 are subtracted [15].

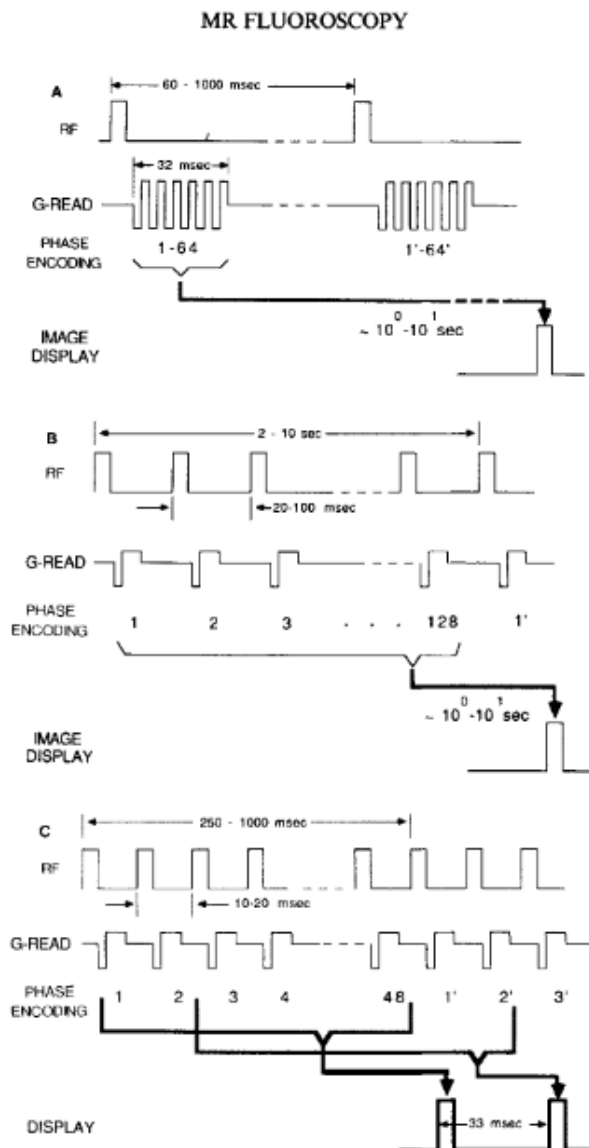


Figure 4
Pulse sequences for standard echo planar imaging (A), SPGR sequence (B), and sliding window real-time acquisitions (C) [15]

Phantom Model

The navigation was tested in a simplified abdominal aorta phantom model made of polyvinyl alcohol cryogel (Sevol Grade 165 PVA powder, Sekisui Specialty Chemicals America, Dallas, TX) and described by Moftakhar and colleagues in their 2015 paper. The different branches off the aorta were constructed with Delrin rods (McMaster-Carr, Elmhurst, IL) to

simulate physiologically accurate branch angles and directions. The phantom contains simulated anatomic geometries of the celiac artery with a diameter of 8mm at 60 degrees from aorta, the superior mesenteric artery (SMA) with a diameter of 8mm at 50 degrees from the aorta, bilateral renal arteries with diameters of 6mm at 60 degrees from the aorta, and the inferior mesenteric artery (IMA) with a diameter of 6mm at 60 degrees from the aorta. After the cryogel set, the Delrin rods were removed and the phantom was submerged in water. An MRI-safe 15-F Check-Flo Performance Introducer (Cook, Bloomington, IN) was used to mimic vascular access to the aorta. Figure 5 is a schematic of the phantom in a coronal section with two renal arteries branching on the left and right.



Figure 5
Schematic of a coronal section of the phantom used.

MRI Guidance Procedures

To assess the viability of using the new EPflex guidewire under MRI-guidance, we measured the success rate of navigation into a phantom artery using the EPflex wire and Cook Beacon 5 Fr vertebral catheter (Cook, Bloomington, IN). In RTHawk, a balanced steady state free precession (bSSFP) real-time sequence with a slice thickness of 15mm, a flip angle of 21 degrees, and 31cm field of view (FOV) was used. The acquisition matrix was 133 by 133, and

the resulting image resolution was 2.3mm². A 15mm slice thickness was used to ensure the guidewire and catheter remained in the visualization frame. The framerate of this real-time sequence was 32msec/image. Navigation was performed at 3.0T (Discovery MR 750w, GE Healthcare, Chicago, IL). Each navigator was given five minutes of proctored practice before recording an attempt to familiarize themselves with the environment and procedures. Every attempted navigation “run” required the operator to advance the wire from the base of the phantom and to turn the guidewire into both phantom renal arteries on the left or the right of the phantom aorta. A success was denoted as a time less than 60 seconds to gain access to the renal artery and a failure was denoted as a time greater than 60 seconds to gain access to the renal artery. Each operator attempted 10 runs on each renal artery for a total of 20 attempts per operator per imaging modality. In addition to collection of success/failure rates, total time to navigate into the vessel was also collected. Each operator was given the choice to navigate into each renal artery for 10 attempts consecutively or alternate between renals; the only condition being consistency in approach when testing each imaging modality. Two experienced attending neurointerventional radiologists at the University of California, San Francisco Medical Center and two inexperienced operators recorded runs.

An 8-channel cardiac array coil was used. After the localizer was performed, remote access to a second computer running RTHawk was gained via a program called VNC Viewer (RealVNC, Cambridge, UK) on a personal laptop (MacBook Air, Apple, Cupertino, CA) which allowed remote control of a given computer. Once the RTHawk computer was accessed through VNC Viewer, RTHawk was opened and the SSFP real-time sequence was initiated with the above parameters. An MRI-safe and RF shielded power cable and optical cable was connected

from the personal laptop to a projection monitor (NordicNeuroLab LLC, Bergen, Norway) within the MRI suite. A schematic of the MRI setup is shown in Figure 6.

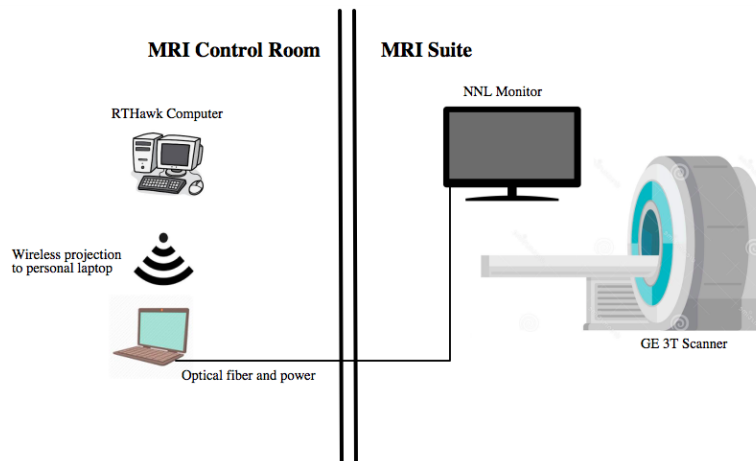


Figure 6
Schematic of MRI setup

X-ray Guidance Procedures

A similar method was used for x-ray guidance. All x-ray navigation was performed on a Siemens Cios Alpha C-arm x-ray fluoroscopy device (Siemens Healthineers AG, Forcheim, Germany) The EPflex MRline guidewire was used with the same vertebral catheter in the same abdominal aorta phantom model. Before any data collection, an injection of Omnipaque 350 (General Electric Healthcare, Waukesha WI) iodinated contrast was injected through the vertebral catheter to distinguish the phantom vessels. Six milliliters of contrast were mixed with six milliliters of tap water and the 12ml solution was administered to the phantom. Additional contrast was added per operator request. Each of the four total operators again attempted 10 turns into each of the phantom renal arteries for 20 total attempts per operator with the EPflex guidewire. The EPflex wire performance under x-ray guidance was also compared to data collected by Moftakhar et al, who employed a 110-cm 4-F UCSF3 Super Torque Catheter

(Cordis, Miami Lakes, FL) and a 150-cm-long 0.035 inch-diameter angled stiff-type Glidewire (Terumo, Somerset, NJ) to be used as a reference. Moftakhar et al used the same phantom and imaging setup.

Statistical Analysis

A linear mixed-effects regression analysis was used to compare x-ray-guided and MRI-guided success rates and mean procedure times. A p-value of 0.05 was used to determine significance. Statistical analyses were performed by using Stata version 13 software (StataCorp, College Station, TX).

Results

The results for all operators are shown in Table 1. Additionally, frames of each imaging modality are shown in figures 7 and 8. A total of 158 renal artery accesses were attempted, with 78 on the left renal artery and 80 on the right renal artery. The two experienced operators recorded a combined 80 attempted renal artery accesses and the inexperienced operators recorded 78 renal artery accesses. The experienced operator overall success rate for both modalities was 88% with a mean procedure time of 22 seconds. The inexperienced operator overall success rate for both modalities was 85% with a mean procedure time of 20 seconds. The experienced MRI-guided success rate was 83% with a mean time of 28 seconds while the inexperienced MRI-guided success rate was 76% with a mean time of 25 seconds. The experienced x-ray-guided success rate was 95% with a mean time of 17 seconds, and the inexperienced x-ray-guided success rate was also 95% with a mean time of 15 seconds. The overall mean procedure time for MRI navigation when pooling both groups was significantly

lower than the x-ray guidance ($p = 0.003$). Additionally, procedure time for MRI guidance was significantly longer than x-ray guidance when pooling the groups ($p < 0.001$).

For both imaging modalities and operator groups, the success rate was lower and the procedure time was longer when navigating into the right renal. For all groups and modalities, the average time for left renal navigation was 16 seconds and average time for right renal navigation was 27 seconds. The success rate for both groups for both modalities are 94% for the left renal and 80% for the right renal artery respectively. It should be noted that “left” and “right” refer to the patient’s left or right side, as per radiological convention i.e. the left renal artery appears on the right side of the image.

Table 1
Results for All Operators

Parameter	Overall	P-value	Left renal	p-value	Right renal	p-value
<u>Percentage Success for all operators*</u>						
MRI Guidance	80 (62/78)		90 (34/38)		70 (28/40)	
X-ray Fluoroscopy Guidance	95 (76/80)	0.003	100 (40/40)	0.030	90 (36/40)	0.021
<u>Procedure Time for all operators**</u>						
MRI Guidance	27 [2]		23 [2]		31 [3]	
X-ray Fluoroscopy Guidance	16 [3]	<0.001	9 [3]	<0.001	23 [4]	0.85

* Percent success data is presented as % (numerator/denominator)

** Procedure time is presented in seconds as mean [SEM]

Table 2
Results for Experienced Operators

Parameter	Overall	P-value	Left renal	p-value	Right renal	p-value
<u>Percentage Success for experienced operators</u>						
MRI Guidance	83 (33/40)		90 (19/20)		70 (14/20)	
X-ray Fluoroscopy Guidance	95 (38/40)	0.071	100 (20/20)	0.305	90 (18/20)	0.102
<u>Procedure Time for experienced operators</u>						
MRI Guidance	28 [3]		22 [3]		34 [4]	
X-ray Fluoroscopy Guidance	17 [4]	0.004	8 [4]	0.001	25 [6]	0.142

* Percent success data is presented as % (numerator/denominator)

** Procedure time is presented in seconds as mean [SEM]

Table 3
Results for Inexperienced Operators

Parameter	Overall	P-value	Left renal	p-value	Right renal	p-value
<u>Percentage Success for inexperienced operators*</u>						
MRI Guidance	76 (29/38)		83 (15/18)		70 (14/20)	
X-ray Fluoroscopy Guidance	95 (38/40)	0.014	100 (20/20)	0.046	90 (18/20)	0.102
<u>Procedure Time for inexperienced operators**</u>						
MRI Guidance	25 [3]		23 [3]		28 [5]	
X-ray Fluoroscopy Guidance	15 [4]	0.015	10 [5]	0.003	22 [7]	0.315

* Percent success data is presented as % (numerator/denominator)

** Procedure time is presented in seconds as mean [SEM]

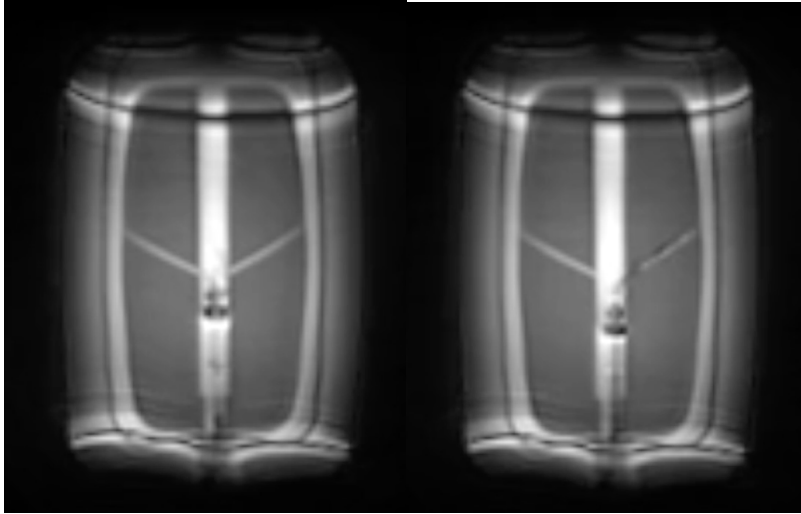


Figure 7

Coronal view of MRI guidance with EPflex wire and vertebral catheter. The left image shows the wire and catheter inside the aorta, and the right image shows wire inside the left renal artery.

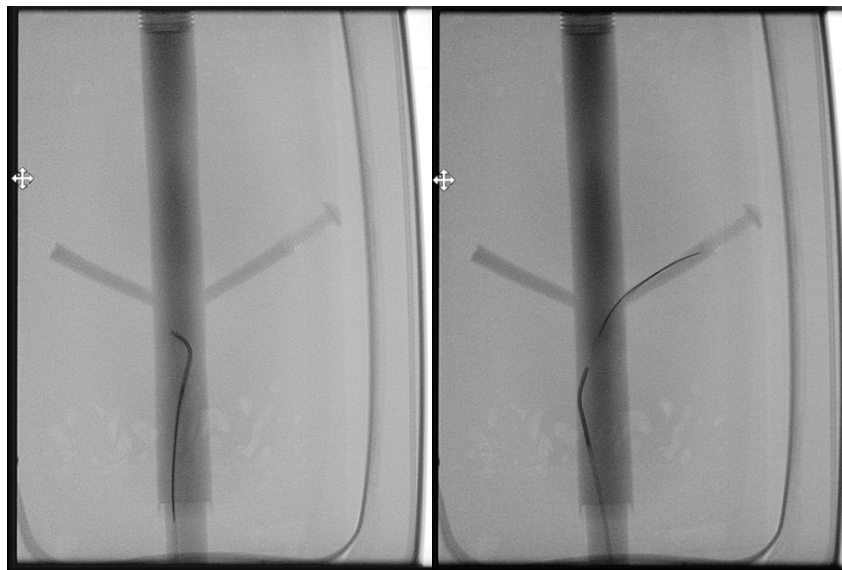


Figure 8

Coronal view of x-ray fluoroscopy guidance with EPflex wire and vertebral catheter. The left image shows the wire and catheter in the aorta, and the right image shows wire inside left renal artery.

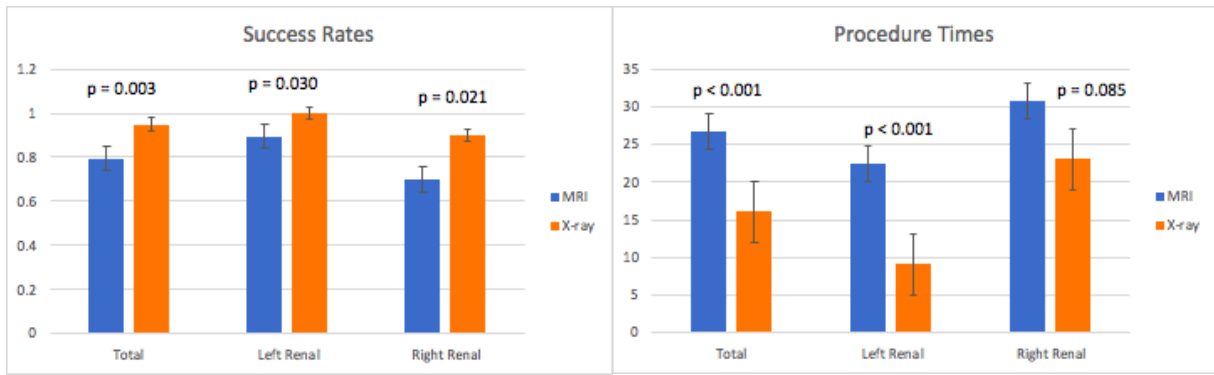


Figure 9

These plots show overall success rates and mean procedure times in seconds

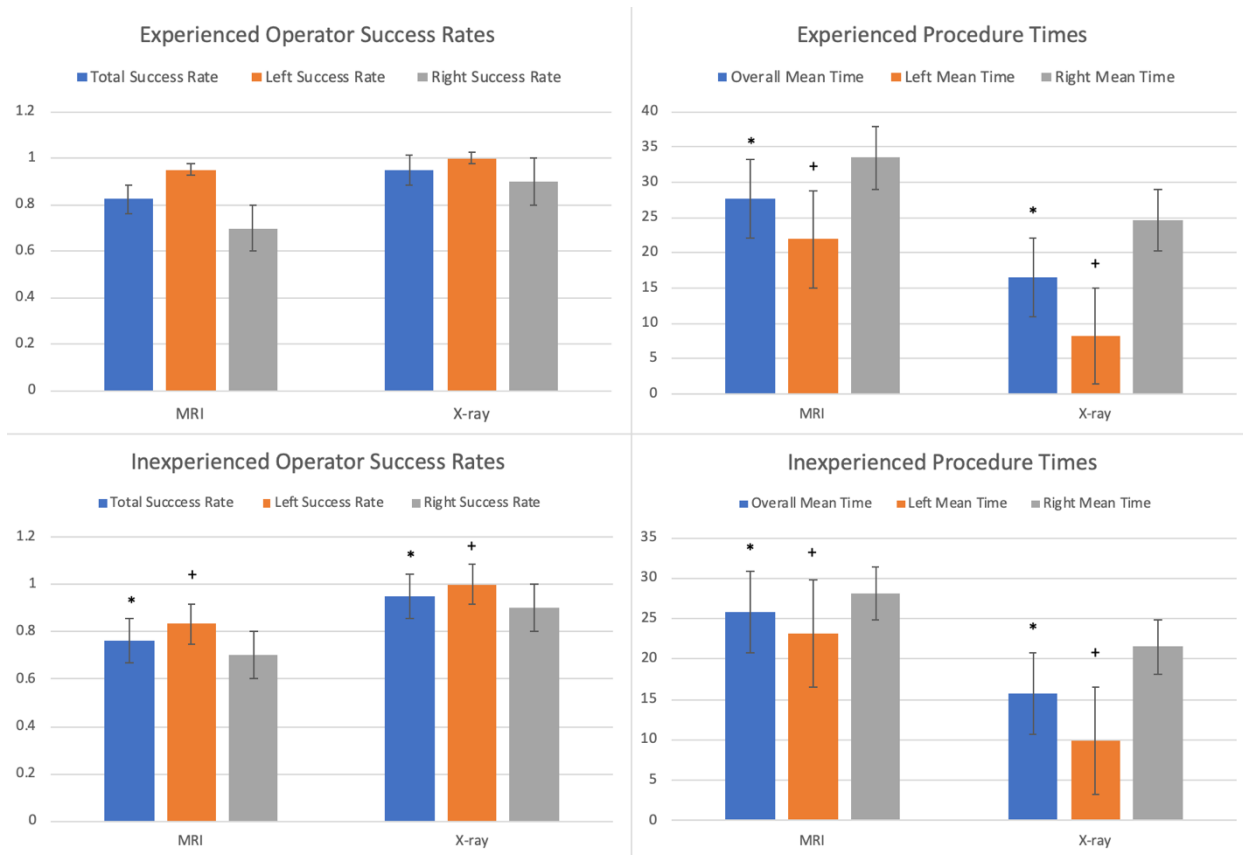


Figure 10

These plots show the success rates and procedure times separated by experienced and inexperienced operators. The asterisk and plus symbols represent statistically significant differences.

Moftakhar et al in 2015 acquired data with a standard Super Torque Catheter and Glidewire guidewire using the same methods and sane phantom. We used their acquired data as a reference. This group achieved an overall x-ray navigation success rate of 86% (69/80) into the renal vessels with the standard guide and catheter. Their reported mean navigation time was 27 seconds for each renal artery for all operators. The EPflex wire and vertebral catheter achieved an overall success rate of 95% (76/80) and mean procedure times of 9 seconds on the left and 16 seconds on the right for x-ray navigation.

Discussion

The EPflex MRline guidewire represents an important step in the direction of developing MRI to guide endovascular treatments. Using MRI would allow clinicians to acquire physiological information in real-time that x-ray imaging cannot provide. Timely acquisition of functional information is particularly critical in the treatment of ischemic stroke where MR diffusion weighted imaging is used to plan the treatment procedure. Acquiring this physiologic information in the same location as the treatment of the stroke saves critical. The EPflex wire is important because it is bridging the transition between x-ray-guided interventions and MRI-guided interventions as it can be used under both guiding modalities. This study demonstrates that, in a phantom model, this wire can be guided with relatively high success under MRI-guidance and shows potential for *in vivo* testing of the wire using MRI.

Overall, x-ray-guided tests were faster and more successful than MRI-guided navigation attempts. This advantage of x-ray can be attributed to the higher spatial and temporal resolution attained with x-ray guidance. It is worth noting that the experienced operators did not see a statistically significant difference in success rate between the two guiding modalities. This suggests that perhaps experienced operators were able to use their familiarity with the tools and

techniques to guide their procedures when the visualization was not as clear. The biggest difficulty in navigating under MRI guidance was the inconsistency with accurately viewing the artifact created by the markers on the wire and catheter. This inconsistency could be due to differing levels of susceptibility artifact from the MRI markers causing signal loss and spatial misaligning. Since susceptibility artifacts are complex manifestations of the pulse sequence and the markers orientation within the static magnetic field, it is possible that marker visibility would vary somewhat during navigation. In addition, the tips may have been hard to visualize at times because the markers were at the edge of the imaging slice. Another possible explanation for the inconsistent visualization is that we observed air bubbles in the catheter which can distort the MR imaging artifact. Clinically, however, air bubbles would not be prevalent in an endovascular procedure because all catheters are connected to saline drips to prevent air bubbles from entering patient circulation.

One notable disadvantage of x-ray guidance was the need to inject iodinated contrast agent to distinguish the vasculature of the phantom. The MRI-guided navigation tests did not need an injection of a contrast agent to visualize these details, and this stands as an important clinical advantage of MRI over x-ray.

The pooled success rate of MRI and x-ray guidance (80% and 95% respectively) are close enough to warrant further examination MRI as a viable guidance modality for endovascular procedures. The difference in overall success rate and mean procedure times between MRI and x-ray may be statistically significant, but this difference may not translate to clinical significance. More studies need to be performed in order to determine whether the differences in success rate and procedure time between x-ray and MRI are of importance in a clinical setting. The present study supports continued testing and development of devices for MRI-guided

procedures since there was an improvement in navigation from Moftakhar and colleagues' results in 2015 with the same phantom. In their similarly designed experiment with the exact same phantom, Moftakhar et al reported 55% and 50% successful navigation in the left and right renal arteries respectively under MRI guidance. In the present experiment, we report 90% and 70% successful navigation attempts in the left and right renal respectively under MRI guidance. This marked improvement of the success rate for navigation into phantom renal arteries from the Moftakhar et al. paper demonstrate improvements in both the instruments used in interventional MRI with the EPflex wire and with real-time MRI software. This leads to the conclusion that using MRI as the guiding modality for endovascular procedures is getting more realistic.

This study was limited by the simplicity of the phantom model. The model did not simulate motion or blood flow, and the modeled vessels are different from physiological ones. This study was also limited in its statistical power because only four operators recorded runs and there were only 158 total data points on which to perform analysis. Another possible limitation includes the order in which operators recorded their data. For example, there could have been a difference in success rate if an operator recorded x-ray data before MRI data and was able to see the phantom in greater detail before the MRI guidance. Similarly, another limitation was allowing the operators to choose between alternating navigation attempts between renal arteries attempting a single renal consecutively. Furthermore, there appeared to be an inconsistency on the inside of the phantom on the right renal side that made it more difficult to navigate into the right renal branch. This discrepancy on the right renal side is reflected in the data. One final limitation of this study could have been batch effect with the wires and catheter. The wires were checked for defects and replaced if necessary for every session, but the same catheter was used

for the entire experiment. Also, it is possible that the phantom model could have changed or been damaged throughout the course of the experiment.

For future examination, it would be valuable to explore navigation using a more complex phantom to test navigation from more operators to gain statistical power. Additionally, it would be interesting to examine navigation efficacy using different MRI guidance software with different scanning parameters. Lastly, *in vivo* testing of the EPflex wire under MRI guidance would be important in evaluating this treatment protocol for safety and efficacy.

Conclusion

Navigation of a vascular phantom was found to be statistically faster and more successful under x-ray guidance than MRI guidance. However, MRI-guided navigation provided a fairly high success rate of 80% which is high enough to warrant continued exploration of MRI as the guiding imaging modality for endovascular procedures. Despite being slightly slower and less successful, there were definitive advantages of MRI primarily because no injected contrast was needed and there was no ionizing radiation. More tests need to be conducted to determine whether the challenges of an MRI environment are outweighed by the potential benefits. The EPflex wire and improved real-time MRI software from RTHawk represent an important step towards the development of clinically useful and effective guidance by MRI. This project had direct clinical applications as the development of safer, more effective endovascular guidance mechanisms is investigated.

References

1. Yaras, Y. S., Satir, S., Ozsoy, C., Ramasawmy, R., Campbell-Washburn, A., Lederman, R., ... Degertekin, L. (2018). Acousto-optic Catheter Tracking Sensor for Interventional MRI Procedures. *IEEE Transactions on Biomedical Engineering*, 66(4), 1148–1154.
<https://doi.org/10.1109/TBME.2018.2868830>
2. Rube, M. A., Holbrook, A. B., Cox, B. F., Houston, J. G., & Melzer, A. (2014). Wireless MR tracking of interventional devices using phase-field dithering and projection reconstruction. *Magnetic Resonance Imaging*, 32(6), 693–701.
<https://doi.org/10.1016/j.mri.2014.03.007>
3. Glowinski, A., Kursch, J., Adam, G., Bucker, A., Noll, T., & Gunther, R. (1998). Device visualization for interventional MRI using local magnetic fields: Basic theory and its application to catheter visualization. *IEEE Transactions on Medical Imaging*, 17(5), 786-793. doi:10.1109/42.736037
4. Ratnayaka, K., Faranesh, A. Z., Hansen, M. S., Stine, A. M., Halabi, M., Barbash, I. M., ... Lederman, R. J. (2013). Real-time MRI-guided right heart catheterization in adults using passive catheters. *European Heart Journal*, 34(5), 380–388.
<https://doi.org/10.1093/eurheartj/ehs189>
5. Serfaty, J., Yang, X., Aksit, P., Quick, H. H., Solaiyappan, M., & Atalar, E. (2000). Toward MRI-guided coronary catheterization: Visualization of guiding catheters, guidewires, and anatomy in real time. *Journal of Magnetic Resonance Imaging*, 12(4), 590-594. doi:10.1002/1522-2586(200010)12:43.0.co;2-3
6. Moftakhar, P., Lillaney, P., Losey, A. D., Cooke, D. L., Martin, A. J., Thorne, B. R., . . . Hetts, S. W. (2015). New-Generation Laser-lithographed Dual-Axis Magnetically

- Assisted Remote-controlled Endovascular Catheter for Interventional MR Imaging: In Vitro Multiplanar Navigation at 1.5 T and 3 T versus X-ray Fluoroscopy. *Radiology*, 277(3), 842-852. doi:10.1148/radiol.2015142648
7. Desai, M. Y., Lardo, A. C., & Lima, J. A. C. (2010). Interventional Cardiovascular MRI. *Interventional Cardiology*, 405–423. <https://doi.org/10.1385/1-59259-898-6:405>
 8. Rogers, T., & Lederman, R. J. (2019). Interventional Cardiovascular MRI. *Contemporary Cardiology Cardiovascular Magnetic Resonance Imaging*, 419-437. doi:10.1007/978-1-4939-8841-9_23
 9. Miller, D. L., Balter, S., Cole, P. E., Lu, H. T., Berenstein, A., Albert, R., . . . Anderson, J. (2003). Radiation Doses in Interventional Radiology Procedures: The RAD-IR Study Part II: Skin Dose. *Journal of Vascular and Interventional Radiology*, 14(8), 977-990. doi:10.1097/01.rvi.0000084601.43811.cb
 10. Uecker, M., Zhang, S., Voit, D., Karaus, A., Merboldt, K. D., & Frahm, J. (2010). Real-time MRI at a resolution of 20 ms. *NMR in Biomedicine*, 23(8), 986–994. <https://doi.org/10.1002/nbm.1585>
 11. Guide Wires | Nitinol & Stainless Steel | CE-Certified. (n.d.). Retrieved from <https://www.epflex.com/en/products/mrline/>
 12. Le-Bihan, D., Mangin C, J., Clark, C., Pappata, S., Molko, N., & Chabriat, H. (2001). Diffusion tensor imaging: Concepts and applications. *Journal of Magnetic Resonance Imaging*, 13(4), 534–546.
 13. Campbell-Washburn, A. E., Faranesh, A. Z., Lederman, R. J., & Hansen, M. S. (2015). Magnetic Resonance Sequences and Rapid Acquisition for MR-Guided Interventions.

Magnetic Resonance Imaging Clinics of North America, 23(4), 669–679.

<https://doi.org/10.1016/j.mric.2015.05.006>

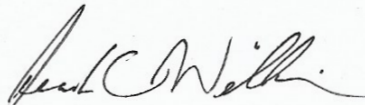
14. Santos, J. M., Wright, G. A., & Pauly, J. M. (2005). Flexible real-time magnetic resonance imaging framework. The 26th Annual International Conference of the IEEE Engineering in Medicine and Biology Society, 1, 1048–1051.
<https://doi.org/10.1109/iembs.2004.1403343>
15. Riederer, S. J., Tasciyan, T., Farzaneh, F., Lee, J. N., Wright, R. C., & Herfkens, R. J. (1988). MR fluoroscopy: Technical feasibility. Magnetic Resonance in Medicine, 8(1), 1–15. <https://doi.org/10.1002/mrm.1910080102>
16. Moseley ME, Cohen Y, Mintorovitch J. Early detection of regional cerebral ischemic injury in cats: evaluation of diffusion and T2- weighted MRI and spectroscopy. Magn Reson Med 1990;14:330– 346.
17. Zerna, C., Assis, Z., D’Esterre, C. D., Menon, B. K., & Goyal, M. (2016). Imaging, intervention, and workflow in acute ischemic stroke: The calgary approach. American Journal of Neuroradiology, 37(6), 978–984. <https://doi.org/10.3174/ajnr.A4610>

Publishing Agreement

It is the policy of the University to encourage the distribution of all theses, dissertations, and manuscripts. Copies of all UCSF theses, dissertations, and manuscripts will be routed to the library via the Graduate Division. The library will make all theses, dissertations, and manuscripts accessible to the public and will preserve these to the best of their abilities, in perpetuity.

Please sign the following statement:

I hereby grant permission to the Graduate Division of the University of California, San Francisco to release copies of my thesis, dissertation, or manuscript to the Campus Library to provide access and preservation, in whole or in part, in perpetuity.



Author Signature

10/8/19

Date